

# Computer Design of Living Olefin Polymerization Catalysts: A Combined Density Functional Theory and Molecular Mechanics Study

Liqun Deng,<sup>†</sup> Tom Ziegler,<sup>\*,†</sup> Tom K. Woo,<sup>†</sup> Peter Margl,<sup>†</sup> and Liangyou Fan<sup>‡</sup>

Department of Chemistry, The University of Calgary, Calgary, Alberta T2N 1N4, Canada, and  
Novacor Research and Technology Corporation, 2928-16 Street NE,  
Calgary, Alberta T2E 7K7, Canada

Received April 24, 1998

Ethylene polymerization catalyzed by group-4 diamide complexes has been studied by molecular modeling. The modeling was based on pure density functional theory (DFT) in the case of the generic  $[\text{RNCH}_2\text{CH}_2\text{CH}_2\text{NR}]\text{MCH}_2\text{CH}_2\text{CH}_3^+$  complexes with  $\text{R} = \text{H}$  and  $\text{M} = \text{Ti}$ ,  $\text{Zr}$ , and  $\text{Hf}$ . For the substituted systems with  $\text{R} = 2,6\text{-}^i\text{Pr}_2\text{C}_6\text{H}_3$  and  $\text{M} = \text{Ti}$  and  $\text{Zr}$ , a combined DFT and molecular mechanics (MM) scheme (QM/MM) was employed. The generic systems revealed the following trends with respect to the three group-4 metals: ethylene complexation energies are  $\text{Ti}$  (19.2 kcal/mol) <  $\text{Hf}$  (21.3 kcal/mol)  $\leq$   $\text{Zr}$  (22.0 kcal/mol); the overall insertion barriers  $\Delta E_{\text{insertion}}^\ddagger$  are  $\text{Zr}$  (7.4 kcal/mol)  $\leq$   $\text{Ti}$  (8.1 kcal/mol) <  $\text{Hf}$  (9.6 kcal/mol); and the chain termination barriers,  $\Delta E_{\text{termination}}^\ddagger$ , relative to the most stable  $\pi$  complexes are  $\text{Hf}$  (8.1 kcal/mol)  $\approx$   $\text{Zr}$  (8.2 kcal/mol) <  $\text{Ti}$  (10.3 kcal/mol). The QM/MM calculations on the substituted systems gave the following energies: for ethylene complexation 17.0 (Ti) and 22.4 (Zr) kcal/mol; for the insertion barriers 9.4 (Ti) and 11.8 (Zr) kcal/mol; and for the chain termination barriers 19.2 (Ti) and 11.7 (Zr) kcal/mol. The calculated ratio for the rate of insertion versus termination ( $\Delta E_{\text{termination}}^\ddagger - \Delta E_{\text{insertion}}^\ddagger$ ) are 42:1 (Ti), 6:1 (Zr), 1:13 (Hf) for  $\text{R} = \text{H}$  and 20 000 000:1 (Ti) and 1:1 (Zr) for  $\text{R} = 2,6\text{-}^i\text{Pr}_2\text{C}_6\text{H}_3$ . The differences in the predicted performance of the substituted systems for titanium and zirconium are in agreement with experimental findings by McConville et al. The poor performance of the zirconium catalyst is rationalized. On the basis of this analysis, new zirconium catalysts are suggested with increased steric bulk on the diamide chain or the aryl groups. The new complexes were shown by QM/MM calculations to be potential living polymerization catalysts with higher activity than the titanium diamide systems suggested by McConville et al.

## I. Introduction

Olefin polymerization catalysts composed of a group-4 metallocene complex have been developed to a high degree of sophistication over the past decade as alternatives to the classical Ziegler–Natta systems comprised of titanium halides and alkyl aluminum.<sup>1–5</sup> More recently, the search for single-site catalysts has been extended beyond group-4 metallocenes in the hope of achieving superior polymer specifications and lower production costs. Special attention has been given to chelating diamide complexes of group-4 metals<sup>6–9</sup> as well as  $\text{Ni(II)}$ - and  $\text{Pd(II)}$ -based diimine compounds.<sup>10,11</sup>

An important development in the search for new single-site systems has been the discovery by McConville et al.<sup>6</sup> of a titanium diamide complex that can serve as a living catalyst for the polymerization of  $\alpha$ -olefins, although the activity is relatively low. A key to the success of this system is the presence of bulky substituents on the chelating nitrogen atoms. Interestingly,

the corresponding zirconium system does not polymerize olefins. This is surprising since the first generation of single-site metallocene catalysts in most cases exhibit a larger activity for zirconium than for titanium.

The objective of the present investigation is to understand why the McConville-type<sup>6</sup> titanium diamide complexes are living catalysts while titanocenes and the homologous zirconium diamide systems are not. We will also suggest modifications of the steric bulk on the chelating nitrogen atoms which, according to our calculations, make the modified zirconium analogue both living and highly active. Our investigation will build on experience gained in a recent computational study<sup>12,13</sup>

(6) Scollard, J. D.; McConville, D. H. *J. Am. Chem. Soc.* **1996**, *118*, 10008.

(7) Scollard, J. D.; McConville, D. H.; Payne, N. C.; Vittal, J. *Macromolecules* **1996**, *29*, 5241.

(8) Baumann, R.; Davis, W. M.; Schrock, R. R. *J. Am. Chem. Soc.* **1997**, *119*, 3830.

(9) Warren, T. H.; Schrock, R. R.; Davis, W. M. *Organometallics* **1996**, *15*, 562.

(10) Johnson, L. K.; Killian, C. M.; Brookhart, M. *J. Am. Chem. Soc.* **1995**, *117*, 6414.

(11) Johnson, L. K.; Mecking, S.; Brookhart, M. *J. Am. Chem. Soc.* **1996**, *118*, 267.

(12) Deng, L.; Margl, P. M.; Ziegler, T. *J. Am. Chem. Soc.* **1997**, *119*, 1094.

<sup>†</sup> The University of Calgary.

<sup>‡</sup> Novacor Research and Technology Corp.

(1) Ewen, J. A. *Sci. Am.* **1997**, *276*(5), 86.

(2) Haggin, J. *Chem. Eng. News* **1996**, *74*(6), 6.

(3) Thayer, A. M. *Chem. Eng. News* **1995**, *73*(37), 15.

(4) Bochmann, M. *J. Chem. Soc., Dalton Trans.* **1996**, 255.

(5) Brintzinger, H. H.; Fischer, D.; Muelhaupt, R.; Waymouth, R. M. *Angew. Chem., Int. Ed. Engl.* **1995**, *34*, 1143.

of the Ni(II) diimine olefin polymerization catalyst due to Brookhart et al.<sup>11</sup>

The discussion will be split into three parts. The first examines the electronic differences between the generic titanium, zirconium, and hafnium systems where the bulky substituents on nitrogen have been replaced by hydrogen atoms. The second part analyzes the role played by the bulky ligands in the living titanium-based McConville catalyst as well as the reason for the poor polymerization performance of the zirconium homologue. The analysis here will be based on a combined density functional theory (DFT) and molecular mechanics (MM) approach.<sup>13–15</sup> Finally, we will make use of our findings above to suggest modifications of the bulky substituents on the chelating nitrogens. The resulting zirconium diamide complexes have, according to our calculations, the potential to be living olefin polymerization catalysts. Experimental confirmation of the polymerization characteristics of these new catalysts are currently underway by Piers et al.<sup>58</sup>

## II. Computational Details

All reported DFT calculations were performed by means of the Amsterdam Density Functional (ADF) program system, developed by Baerends<sup>16,17</sup> et al. and vectorized by Ravenek.<sup>18</sup> The numerical integration scheme applied for the calculations was developed by te Velde<sup>19</sup> et al. The geometry optimization procedure was based on the method of Versluis and Ziegler.<sup>20</sup> The electronic configurations of the molecular systems were described by a triple- $\zeta$  basis set<sup>21,22</sup> on the metal centers for the *ns*, *np*, *nd*, (*n* + 1)*s*, and (*n* + 1)*p* valence shells. A double- $\zeta$  STO basis set was used for carbon (2*s*, 2*p*), hydrogen (1*s*), and nitrogen (2*s*, 2*p*), augmented with a single 3*d* polarization function except for hydrogen where a 2*p* function was used. The inner shells on the metals as well as carbon and nitrogen were treated within the frozen core approximation. A set of auxiliary<sup>23</sup> *s*, *p*, *d*, *f*, and *g* STO functions, centered on all nuclei, was used in order to fit the molecular density and present Coulomb and exchange potentials accurately in each SCF cycle. Energy differences were calculated by augmenting the local exchange-correlation potential by Vosko<sup>24</sup> et al. with Becke's<sup>25</sup> nonlocal exchange corrections and Perdew's<sup>26,27</sup> nonlocal correlation corrections. Geometries were optimized including nonlocal corrections. First-order (FO) scalar relativistic corrections<sup>28,29</sup> were added to the total energy for titanium and zirconium, whereas hafnium was treated by a

quasi-relativistic (QR) approach.<sup>30,31</sup> For the purpose of verifying the perturbative relativistic approach for the lighter metal centers, QR calculations<sup>30,31</sup> were also carried out for the model zirconium complexes. In view of the fact that all systems investigated in this work show a large HOMO–LUMO gap, a spin-restricted formalism was used for all calculations.

The ADF program system was modified<sup>15</sup> to include the AMBER95<sup>32</sup> molecular mechanics force field in such a way that the QM(DFT) and MM parts are coupled self-consistently, according to the method prescribed by Maseras and Morokuma.<sup>14</sup> In the combined QM/MM calculations, the QM part consisted of the generic complex in which the substituents on the nitrogen atoms were replaced by hydrogen atoms. The actual bulky aryl groups attached to the nitrogens were treated by the pure MM method. The QM and MM parts were linked by the generic hydrogen atoms and coupled by van der Waals interactions. The geometry optimization on the entire system was carried out with coupling between QM and MM atoms. In the optimization of the MM part, the N–C(aryl) distances were constrained to be 0.32 Å longer than the optimized N–H(generic) distance.

An augmented AMBER95 force field<sup>32</sup> was utilized to describe the molecular mechanics potential. (All force field parameters are provided as Supporting Information.) Employing the AMBER atom-type labels as described in ref 32, the diamide carbon was assigned with atom-type "CT" parameters, the diamide N with "N2", aryl ring carbon atoms with "CA", aryl ring hydrogen atoms with "HA", and the remaining carbon and hydrogen atoms of the MM region with "CT" and "HC", respectively. For the propagation and termination processes, the reacting ethylene monomer was assigned with *sp*<sup>2</sup> "C" van der Waals parameters through to the transition-state structure and changed to *sp*<sup>3</sup> "CT" parameters in the product. Alkyl carbon and hydrogen atoms of the active site were assigned "CT" and "HC" van der Waals parameters, respectively. Titanium and zirconium were assigned, respectively, the "Ti3 + 4" and "Zr3 + 4" van der Waals parameters of Rappé's universal force field (UFF).<sup>33</sup> Electrostatic interactions were not included in the molecular mechanics potential. The justification for this approach has been discussed in our previous paper.<sup>13</sup>

It is known that the McConville system only performs in a living fashion when used in conjunction with large borate counterions, which are created in the catalyst activation process where a methyl group is abstracted from the titanium center by a triphenyl borane derivative BR<sub>3</sub>, resulting in a CH<sub>3</sub>BR<sub>3</sub><sup>–</sup> ion. The R groups on the counterion are sterically bulky and, thus, make it unlikely that the counterion can block the active metal site once the alkyl chain is growing and long enough to impair the counterion's access to the metal by entanglement. The primary driving force for the ion-pair formation and, thus, active-site blocking is electrostatics. As electrostatics is both nondirectional and long-range, it is likely that the ion pair is formed in such a manner that the counterion does not sit in the most constricted space on the catalyst, namely the active site. We shall, therefore, assume that neglecting the counterion does not significantly alter the conclusions drawn in the present study.

All structures shown correspond to minimum points on the potential surface, except those prefixed by TS, which represent transition states. Transition states were fully optimized using

(13) Deng, L.; Woo, K. T.; Cavallo, L.; Margl, P.; Ziegler, T. *J. Am. Chem. Soc.* **1997**, *119*, 6177.

(14) Maseras, F.; Morokuma, K. *J. Comput. Chem.* **1995**, *16*, 1170.

(15) Woo, T. K.; Cavallo, L.; Ziegler, T. Unpublished work.

(16) Baerends, E. J.; Ellis, D. E.; Ros, P. *Chem. Phys.* **1973**, *2*, 41.

(17) Baerends, E. J.; Ros, P. *Chem. Phys.* **1973**, *2*, 52.

(18) *Algorithms and Applications on Vector and Parallel Computers*; Ravenek, W., Ed.; Elsevier: Amsterdam, The Netherlands, 1987.

(19) te Velde, G.; Baerends, E. J. *J. Comput. Chem.* **1992**, *99*, 84.

(20) Versluis, L.; Ziegler, T. *J. Chem. Phys.* **1988**, *88*, 322.

(21) Snijders, J. G.; Baerends, E. J.; Vernois, P. *At. Nucl. Data Tables* **1982**, *26*, 483.

(22) Vernois, P.; Snijders, J. G.; Baerends, E. J. *Slater Type Basis Functions for the Whole Periodic System*; Internal report (in Dutch); Department of Theoretical Chemistry, Free University: Amsterdam, The Netherlands, 1981.

(23) Krijn, J.; Baerends, E. J. *Fit Functions in the HFS Method*; Internal Report (in Dutch); Department of Theoretical Chemistry, Free University: Amsterdam, The Netherlands, 1984.

(24) Vosko, S. H.; Wilk, L.; Nusair, M. *Can. J. Phys.* **1980**, *58*, 1200.

(25) Becke, A. *Phys. Rev. A* **1988**, *38*, 3098.

(26) Perdew, J. P.; Zunger, A. *Phys. Rev. B* **1981**, *23*, 5048.

(27) Perdew, J. P. *Phys. Rev. B* **1986**, *33*, 8822.

(28) Snijders, J. G.; Baerends, E. J. *Mol. Phys.* **1978**, *36*, 1789.

(29) Snijders, J. G.; Baerends, E. J.; Ros, P. *Mol. Phys.* **1979**, *38*, 1909.

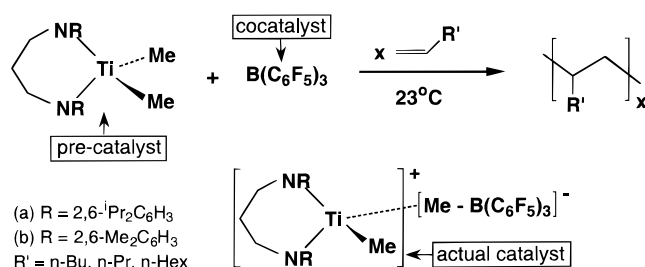
(30) Schreckenbach, G.; Li, J.; Ziegler, T. *Int. J. Quantum Chem.* **1995**, *56*, 477.

(31) Ziegler, T.; Snijders, J. G.; Baerends, E. J. *J. Chem. Phys.* **1981**, *74*, 1271.

(32) Cornell, W. D.; Cieplak, P.; Bayly, C. I.; Gould, I. R.; Merz, K. M., Jr.; Ferguson, D. M.; Spellmeyer, D. C.; Fox, T.; Caldwell, J. W.; Kollman, P. A. *J. Am. Chem. Soc.* **1995**, *117*, 5179.

(33) Rappé, A. K.; Casewit, C. J.; Colwell, K. S.; Goddard, W. A., III; Skiff, W. M. *J. Am. Chem. Soc.* **1992**, *114*, 10024.

Scheme 1



the algorithm of Banerjee et al.,<sup>34,35</sup> starting from the structures obtained by linear transit calculations. No symmetry constraints were used. We have recently verified the accuracy of our DFT approach in a very similar Pd(II) system, where the barrier heights were found to be within 3–5 kcal/mol of experimental estimates.<sup>36,37</sup> Stanton and Merz have undertaken a systematic study of the reliability of DFT calculations for barrier heights and have concluded that DFT yields results of the same quality as post-HF calculations.<sup>38</sup> In a number of previous papers, transition-metal–ligand dissociation energetics have been shown to be correct to within 5 kcal/mol of the experimental values.<sup>39–43</sup> Robb and co-workers<sup>63</sup> have recently reported that the Becke88–Perdew86 exchange correlation functional used in this study provided superior results for complexation energies and vibrational frequencies for a series of Ni olefin complexes compared to other pure density functionals and hybrid density functionals. The combined or integrated QM/MM method has recently been applied to organometallic systems in our group<sup>13</sup> and by Morokuma and co-workers.<sup>44</sup>

### III. Results and Discussion

**A. General Considerations.** Scollard and McConville have already shown<sup>6,45</sup> that the actual catalyst in the living polymerization of 1-hexene by titanium diamide is the cationic species [ArNCH<sub>2</sub>CH<sub>2</sub>CH<sub>2</sub>NAr]<sup>+</sup>MR<sup>−</sup>, where M = Ti and Ar = 2,6-<sup>i</sup>Pr<sub>2</sub>-C<sub>6</sub>H<sub>3</sub>, Scheme 1. However, they did not provide the mechanistic details for the polymerization processes.

Here we adapt the generally accepted Cossée–Arlman mechanism<sup>46,47</sup> (Scheme 2) in our modeling of the group-4 diamide-catalyzed polymerization processes. According to this mechanism, the chain propagation starts from an olefin attacking the metal center to form a  $\pi$ -complex, followed by migratory insertion of the olefin into the M–R bond.

The polymer length is determined by the difference in rate between chain propagation (insertion) and chain termination. A number of different mechanisms have been suggested for the termination process<sup>4–6,46–48</sup> such

as  $\beta$ -alkyl elimination,  $\beta$ -hydride elimination,  $\beta$ -hydrogen transfer to the monomer, C–H activation on monomer by metathesis with the M–C(polymer) bond, and chain transfer to a cocatalyst. Both chain transfer to a cocatalyst and  $\beta$ -alkyl elimination can be controlled (minimized) experimentally<sup>6,48,49</sup> and will not concern us any further here. Theoretical calculations on ethylene polymerization catalyzed by (CpSiH<sub>2</sub>NH)Ti–R<sup>+</sup><sup>50</sup> have shown that olefinic C–H bond activation by  $\sigma$ -bond metathesis, Scheme 2, has a high activation barrier. We shall, therefore, restrict our study of the termination process to the  $\beta$ -H transfer and elimination mechanisms, Scheme 2. It has been shown that  $\beta$ -H elimination has to be modeled with at least propyl. Therefore, we use it in our modeling.

The cationic alkyl complex [ArNCH<sub>2</sub>CH<sub>2</sub>CH<sub>2</sub>NAr]<sup>+</sup>MR<sup>−</sup> can have two different conformations depending on whether the unique carbon in the chelating diamide ligand is on the same (endo) or opposite side (exo) of the N–M–N plane relative to the  $\beta$ -agostic hydrogen of the growing chain. Further, the incoming olefin may coordinate syn (front) or anti (back) to the  $\beta$ -agostic bond. We have, as a result, four possible conformations for the olefin complex which we will term endo frontside (endo-FS), endo backside (endo-BS), exo frontside (exo-FS), and exo backside (exo-BS), respectively. The energy profiles for the chain propagation and  $\beta$ -H transfer, Scheme 2, will depend on the conformation of the olefin complex from which they commence. On the other hand, the  $\beta$ -H elimination, Scheme 2, will depend on the conformation of the cationic alkyl complex. A detailed discussion of the mechanisms in Scheme 2 and their conformational dependence will be presented in the following sections.

**B. The Generic Systems without Bulky Substituents.** We shall start our study by performing pure DFT calculations on a model of the McConville catalyst in which the bulky diamide ArNCH<sub>2</sub>CH<sub>2</sub>CH<sub>2</sub>NAr (Ar = 2,6-<sup>i</sup>Pr<sub>2</sub>-C<sub>6</sub>H<sub>3</sub>) employed by McConville et al. has been replaced by HNCH<sub>2</sub>CH<sub>2</sub>CH<sub>2</sub>NH. Use of the generic model system will allow us to look specifically at the electronic factors. In the next step, the influence of the steric bulk will be studied by reintroducing Ar = 2,6-<sup>i</sup>Pr<sub>2</sub>-C<sub>6</sub>H<sub>3</sub> as the substituents on the chelating nitrogen atoms by using the combined QM/MM technique. A similar two-step approach<sup>12,13</sup> was applied successfully to understand the Ni(II)–diimine catalyst by Brookhart et al.<sup>10,11</sup> Throughout this paper, generic systems with HNCH<sub>2</sub>CH<sub>2</sub>CH<sub>2</sub>NH as the ligand will be referred to by numerals attached to lower-case letters (e.g., **1a**, **2b**, **4c**) whereas numerals attached to upper case letters (e.g., **1A**, **2B**) refer to structures with ArNCH<sub>2</sub>CH<sub>2</sub>CH<sub>2</sub>NAr (Ar = 2,6-<sup>i</sup>Pr<sub>2</sub>-C<sub>6</sub>H<sub>3</sub>) as the ligand, where **a/A**, **b/B**, and **c** represent the titanium, zirconium, and hafnium systems, respectively.

**i. Generic Titanium and Zirconium Systems. Cationic Alkyl Complexes.** Optimized structures for the cationic alkyl complexes [HNCH<sub>2</sub>CH<sub>2</sub>CH<sub>2</sub>NH]MCH<sub>2</sub>–

(34) Banerjee, A.; Adams, N.; Simons, J.; Shepard, R. *J. Phys. Chem.* **1985**, *89*, 52.

(35) Fan, L.; Ziegler, T. *J. Chem. Phys.* **1990**, *92*, 3645.

(36) Margl, P.; Ziegler, T. *Organometallics* **1996**, *15*, 5519.

(37) Margl, P. M.; Ziegler, T. *J. Am. Chem. Soc.* **1996**, *118*, 7337.

(38) Stanton, R. V.; Merz, K. M. *J. J. Chem. Phys.* **1993**, *100*, 434.

(39) Folga, E.; Ziegler, T. *J. Am. Chem. Soc.* **1993**, *115*, 5169.

(40) Li, J.; Schreckenbach, G.; Ziegler, T. *J. Phys. Chem.* **1994**, *98*, 4838.

(41) Li, J.; Schreckenbach, G.; Ziegler, T. *J. Am. Chem. Soc.* **1995**, *117*, 486.

(42) Ziegler, T.; Li, J. *Can. J. Chem.* **1994**, *72*, 783.

(43) Ziegler, T.; Li, J.; Schreckenbach, G. *Inorg. Chem.* **1995**, *34*, 3245.

(44) Matsubara, T.; Maseras, F.; Koga, N.; Morokuma, K. *J. Phys. Chem.* **1996**, *100*, 2573.

(45) Scollard, J. D.; McConville, D. H.; Rettig, S. J. *Organometallics* **1997**, *16*, 1810.

(46) Cossée, P. *J. Catal.* **1964**, *3*, 80.

(47) Arlman, E. J.; Cossee, P. *J. Catal.* **1964**, *3*, 99.

(48) Resconi, L.; Piemontesi, F.; Franciscano, G.; Abis, L.; Fiorani, T. *J. Am. Chem. Soc.* **1992**, *114*, 1025.

(49) Resconi, L.; Jones, R. L.; Rheingold, A. L.; Yap, G. P. A. *Organometallics* **1996**, *15*, 998.

(50) Woo, T. K.; Margl, P. M.; Ziegler, T.; Blochl, P. E. *Organometallics* **1997**, *16*, 3454.



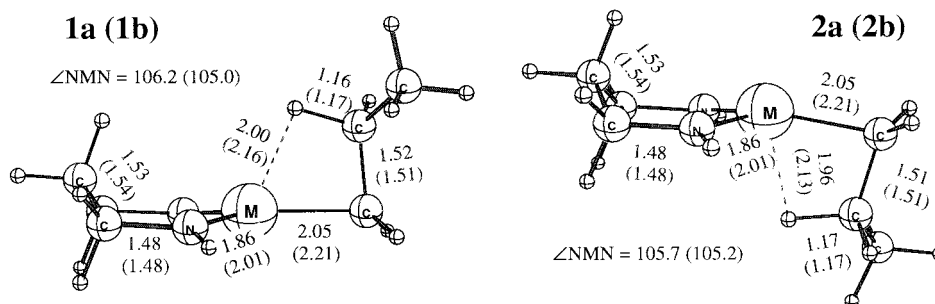
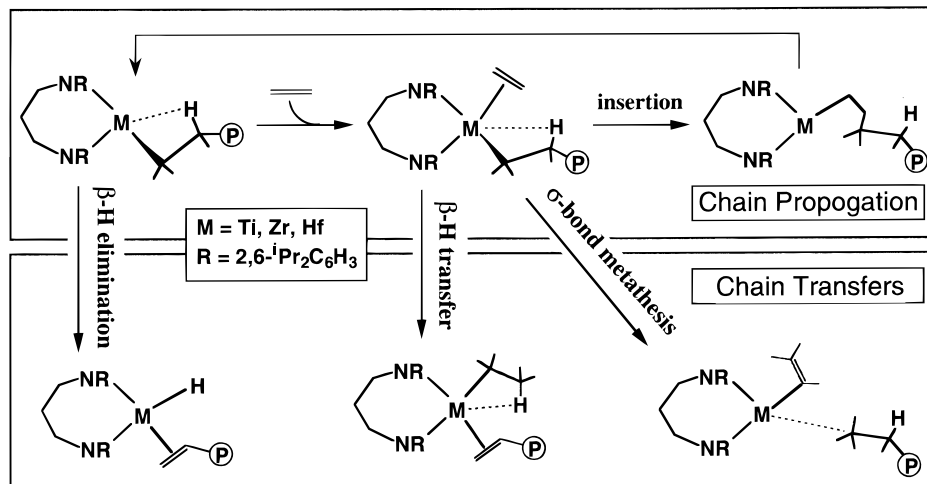


**Figure 1.** Optimized geometries of the metal-alkyl complexes,  $[\text{HN}(\text{CH}_2)_3\text{NH}]\text{MC}_3\text{H}_7^+$ , **1a** (endo,  $\text{M} = \text{Ti}$ ), **1b** (endo,  $\text{M} = \text{Zr}$ ), **2a** (exo,  $\text{M} = \text{Ti}$ ), **2b** (exo,  $\text{M} = \text{Zr}$ ).

**Scheme 2**



$\text{CH}_2\text{CH}_3^+$  are given in Figure 1. Here, **1a** and **2a** refer to the endo and exo conformations, respectively, of the titanium system whereas the corresponding conformations for zirconium are given as **1b** and **2b**, respectively. The two nitrogen atoms are  $\text{sp}^2$  hybridized and coplanar with the metal and the two attached carbon atoms. The metal center adopts a trigonal-planar coordination with respect to the two chelating nitrogens and the bonding  $\alpha$ -carbon of the propyl growing chain. The planar conformations around the metal and the two nitrogens maximizes the stabilizing donation of electron density from the nitrogen lone pairs to empty orbitals on the electron-poor metal center.<sup>51</sup> The secondary agostic interaction between a  $\beta$ -hydrogen on the propyl group and the metal center is seen to take place in an axial position. It follows from Table 1 that the endo and exo conformations of the cationic alkyl complex differ by less than 1 kcal/mol for both titanium and zirconium.

**Complexation of Ethylene to Cationic Alkyl Complexes.** Figure 2 depicts the four conformations for the olefin complex formed by  $\pi$ -complexation of ethylene to the cationic alkyl complex, Scheme 2. The conformations are **3a/3b** (endo-FS), **4a/4b** (endo-BS), **5a/5b** (exo-FS), and **6a/6b** (exo-BS).

As illustrated in Figure 2, the BS conformations can be described as trigonal bipyramidal with the  $\beta$ -hydrogen and ethylene situated in the two axial positions. The original geometry of the cationic alkyl complex is only distorted slightly in the BS conformations **4a/4b** and **6a/6b**, and the  $\beta$ -agostic bond is retained. The distortion

of the cationic alkyl fragment is more noticeable in the FS conformations **3a/3b** and **5a/5b**. Thus, the  $\beta$ -agostic bonds are almost completely ruptured in order to make room for the incoming ethylene. Also, the  $\alpha$ -carbon of the propyl group has been forced out of the trigonal plane. The relative energies for the different conformations are  $-1.4$  (**3a**),  $-3.2$  (**4a**),  $0.0$  (**5a**), and  $-3.8$  kcal/mol (**6a**) for the titanium system and  $-0.4$  (**3b**),  $-1.0$  (**4b**),  $0.0$  (**5b**), and  $-1.8$  kcal/mol (**6b**) for the zirconium system (Table 1). The complexation energies of ethylene in the  $\pi$ -complexes are  $-16.7$  (**3a**),  $-18.5$  (**4a**),  $-15.4$  (**5a**),  $-19.2$  (**6a**),  $-20.6$  (**3b**),  $-21.2$  (**4b**),  $-20.2$  (**5b**), and  $-22.0$  kcal/mol (**6b**). Thus, the larger deformation of the cationic alkyl complex in the FS conformations results in  $\pi$ -complexes that are less stable than the corresponding BS isomers by up to 4 kcal/mol. The energy difference between endo and exo conformations is smaller, with typical values of 1 kcal/mol.

Exo-BS is the conformation of lowest energy for the ethylene complex of both titanium and zirconium, **6a/6b**. The corresponding endo-FS structures can be reached by a rotation of the propyl group around the  $\text{M}-\text{C}(\alpha)$  bond. We estimate the barrier for the rotation to be 0.5 kcal/mol and expect the barrier for exo/endo interconversion by rotation of the alkyl group to be of the same magnitude. Thus, all four conformations of the ethylene  $\pi$ -complex should be available for chain propagation and termination.

**Transition States of Chain Propagation and Termination.** To explore the energetically most favorable channel for chain propagation, we optimized two

(51) Margl, P.; Deng, L.; Ziegler, T. *Organometallics* **1998**, *17*, 933.

**Table 1.** Energetics for the Generic Species Involved in Olefin Polymerization

process and species <sup>a</sup>	energy (kcal/mol)		
	Ti <sup>b</sup>	Zr <sup>c</sup>	Hf <sup>d</sup>
Active Catalyst			
LMC <sub>3</sub> H <sub>7</sub> <sup>+</sup> (endo) ( <b>1a/1b/1c</b> )	0.0	0.0 (0.0)	0.0 (0.0)
LMC <sub>3</sub> H <sub>7</sub> <sup>+</sup> (exo) ( <b>2a/2b/2c</b> )	0.1	0.0 (0.2)	2.1 (1.3)
Endo Ethylene Uptake			
LMC <sub>3</sub> H <sub>7</sub> <sup>+</sup> (endo) ( <b>1a/1b/1c</b> ) + C <sub>2</sub> H <sub>4</sub>	0.0	0.0 (0.0)	0.0 (0.0)
LMC <sub>3</sub> H <sub>7</sub> (C <sub>2</sub> H <sub>4</sub> ) <sup>+</sup> (endo-FS) ( <b>3a/3b/3c</b> )	-16.7	-20.6 (-20.7)	-19.2 (-23.2)
LMC <sub>3</sub> H <sub>7</sub> (C <sub>2</sub> H <sub>4</sub> ) <sup>+</sup> (endo-BS) ( <b>4a/4b/4c</b> )	-18.5	-21.2 (-21.2)	-16.3 (-22.0)
Exo Ethylene Uptake			
LMC <sub>3</sub> H <sub>7</sub> <sup>+</sup> (exo) ( <b>2a/2b/2c</b> ) + C <sub>2</sub> H <sub>4</sub>	0.0	0.0 (0.0)	0.0 (0.0)
LMC <sub>3</sub> H <sub>7</sub> (C <sub>2</sub> H <sub>4</sub> ) <sup>+</sup> (exo-FS) ( <b>5a/5b/5c</b> )	-15.4	-20.2 (-20.4)	-20.3 (-21.5)
LMC <sub>3</sub> H <sub>7</sub> (C <sub>2</sub> H <sub>4</sub> ) <sup>+</sup> (exo-BS) ( <b>6a/6b/6c</b> )	-19.2	-22.0 (-22.2)	-21.3 (-21.9)
Endo-FS Ethylene Insertion			
LMC <sub>3</sub> H <sub>7</sub> (C <sub>2</sub> H <sub>4</sub> ) <sup>+</sup> (endo-FS) ( <b>3a/3b/3c</b> )	0.0	0.0	0.0 (0.0)
TS[ <b>3a-8a</b> ]/[ <b>3b-8b</b> ]/[ <b>3c-8c</b> ]	5.6	6.0 (6.2)	9.6 (8.6)
LMC <sub>3</sub> H <sub>11</sub> <sup>+</sup> ( $\beta$ -agostic) ( <b>7a/7b/7c</b> )	-8.5	-4.6	-4.6 (-2.0)
LMC <sub>3</sub> H <sub>11</sub> <sup>+</sup> ( $\gamma$ -agostic) ( <b>8a/8b/8c</b> )	-8.0	-6.2	-8.4 (-6.7)
LMC <sub>3</sub> H <sub>11</sub> <sup>+</sup> ( $\delta$ -agostic) ( <b>9a/9b/9c</b> ) <sup>e</sup>	-	-5.8	-6.9 (-5.6)
Endo-BS Ethylene Insertion			
LMC <sub>3</sub> H <sub>7</sub> (C <sub>2</sub> H <sub>4</sub> ) <sup>+</sup> (endo-BS) ( <b>4a/4b/4c</b> )	0.0	0.0	0.0
TS[ <b>4a-10a</b> ]/[ <b>4b-10b</b> ]/[ <b>4c-10c</b> ]	7.0	6.4	6.8 (7.5)
$\beta$ -Hydrogen Transfer			
LMC <sub>3</sub> H <sub>7</sub> (C <sub>2</sub> H <sub>4</sub> ) <sup>+</sup> (endo-FS) ( <b>3a/3b/3c</b> )	0.0	0.0	0.0 (0.0)
TS[ <b>3a-11a</b> ]/[ <b>3b-11b</b> ]/[ <b>3c-11c</b> ]	7.8	6.8 (7.0)	8.1 (7.6)
LMC <sub>3</sub> H <sub>6</sub> (C <sub>2</sub> H <sub>5</sub> ) <sup>+</sup> ( <b>11a/11b/11c</b> )	-1.2	-4.6	-3.7 (-3.8)
$\beta$ -Hydrogen Elimination			
LMC <sub>3</sub> H <sub>7</sub> <sup>+</sup> (endo) ( <b>1a/1b/1c</b> )	0.0	0.0	0.0 (0.0)
TS[ <b>1a-12a</b> ]/[ <b>1b-12b</b> ]/[ <b>1c-12c</b> ]	20.1	14.8	17.3 (12.6)
LM(H)(C <sub>2</sub> H <sub>4</sub> ) <sup>+</sup> ( <b>12a/12b/12c</b> )	19.5	11.8	10.1 (8.4)

<sup>a</sup> L = HNCH<sub>2</sub>CH<sub>2</sub>CH<sub>2</sub>NH. <sup>b</sup> Relativistic corrections by first-order perturbation theory. <sup>c</sup> Relativistic corrections by first-order perturbation theory with results from quasi-relativistic calculations in parentheses. <sup>d</sup> Relativistic corrections by quasi-relativistic method with results from first-order relativistic perturbation theory in parentheses. <sup>e</sup> The geometry optimization result showed that **9a** does not exist on the PES.

transition states corresponding to insertion from an endo-FS conformation (front-side insertion), TS[**3a-8a**]/TS[**3b-8b**] of Figure 3, and an endo-BS conformation (back-side insertion), TS[**4a-10a**]/TS[**4b-10b**] of Figure 3, for both titanium and zirconium. The calculations show that TS[**4a-10a**] lies only 0.3 kcal/mol above TS[**3a-8a**] for the titanium system, whereas TS[**4b-10b**] and TS[**3b-8b**] are of nearly the same energy for zirconium (Table 1). With the transition-state energy differences expected to be even smaller between exo and endo conformations, we have decided to restrict our investigation of the propagation and termination processes to a single conformation. We have chosen endo-FS for the  $\pi$ -complex since, in general, any FS complex is a direct precursor to the termination by hydride transfer (Scheme 2). Further, this particular conformation turns out to be the most stable conformation in the substituted system (vide infra). Accordingly, the endo conformation has been chosen for the cationic alkyl complex in connection with ethylene uptake and termination by  $\beta$ -hydrogen elimination, Scheme 2.

Figure 4 displays the TS structures for the termination by hydride transfer, TS[**3a-11a**]/TS[**3b-11b**], as well as  $\beta$ -hydrogen elimination, TS[**1a-12a**]/TS[**1b-12b**]. The kinetic barriers for the titanium systems are 7.8 (TS[**3a-11a**]) and 20.1 kcal/mol (TS[**1a-12a**]) compared to 6.8 (TS[**3b-11b**]) and 14.8 kcal/mol (TS[**1b-12b**]) for the zirconium systems. Thus, hydride transfer is more feasible than  $\beta$ -hydrogen elimination as a termination channel. In fact, the propagation by insertion and termination by hydride transfer have similar activation energies. Thus, the generic diamide systems

based on titanium or zirconium would, at best, be oligomerization catalysts.

A closer look at the TS structures in Figures 3 and 4 reveals that the TS's for hydride transfer, TS[**3a-11a**]/TS[**3b-11b**], are more spatially demanding in the two axial directions than the insertion TS's TS[**3a-8a**]/TS[**3b-8b**]. We shall show in a later section that this observation can be used to suppress termination by increasing steric congestion in the axial directions with bulky substituents on the chelating nitrogens.

**ii. Generic Hafnium System. Influence of the Relativity.** The calculations on titanium and zirconium included only relativistic effects to the first order (FO).<sup>28,29</sup> In this approach, changes in the density induced by relativity are neglected and the geometry is determined from a nonrelativistic calculation. To assess the validity of this approach, all stationary points described above were reoptimized for zirconium within the quasi-relativistic approach (QR)<sup>29-31</sup> in which changes in the density and geometry induced by relativity are taken into account. Furthermore, calculations were carried out at both the QR and the FO levels for the heavier hafnium congener. The results are compared in Table 1.

It follows from Table 1 that relative energies obtained by the FO and QR approaches differ by less than 0.2 kcal/mol for zirconium. For the zirconium system we also find that differences in the geometries are minor, in agreement with the previous findings.<sup>40,41</sup> Thus, first-order perturbation theory is adequate for a description of relativistic effects in elements as heavy as second-row transition metals.

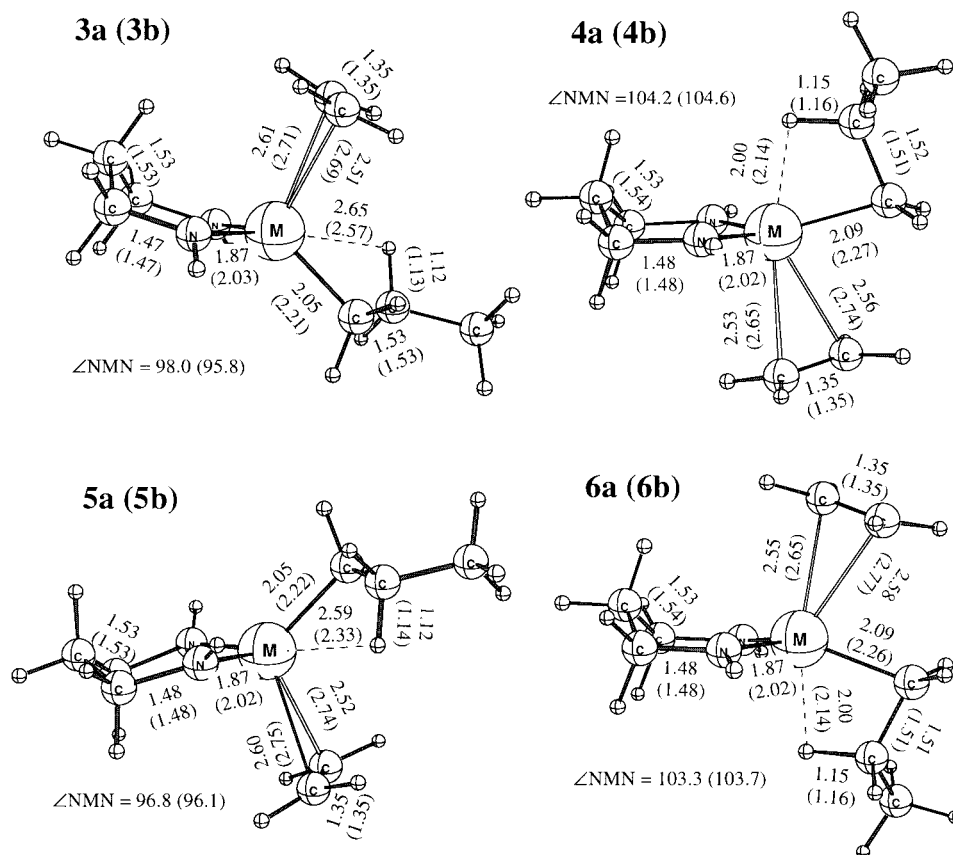


**Figure 2.** Optimized geometries of the metal-alkyl ethylene complexes,  $[\text{HN}(\text{CH}_2)_3\text{NH}]\text{MC}_3\text{H}_7(\text{C}_2\text{H}_4)^+$ , for the titanium system (**3a** (endo-FS), **4a** (endo-BS), **5a** (exo-FS), **6a** (exo-BS)) and for the zirconium systems (**3b** (endo-FS), **4b** (endo-BS), **5b** (exo-FS), **6b** (exo-BS)). Generic systems will be referred to with numerals attached to lower case letters throughout. The letters **a**, **b**, **c** will refer to titanium, zirconium, and hafnium, respectively.

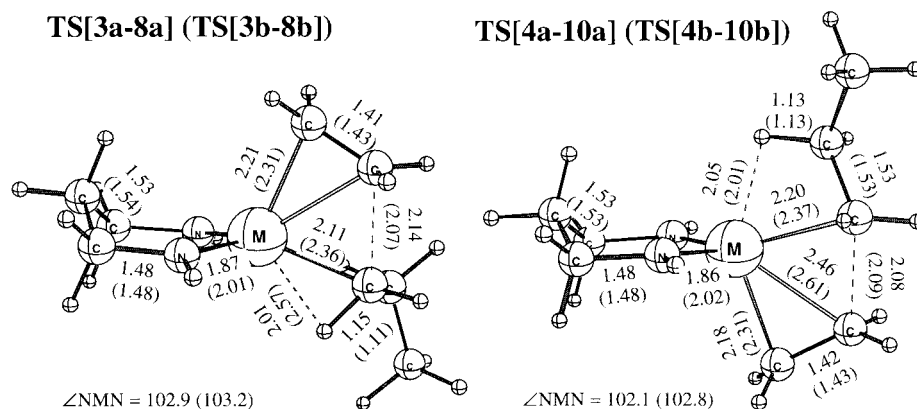


**Figure 3.** Optimized structures for insertion transition states of the titanium and zirconium generic systems. **TS[3a-7a]/TS[3b-8b]** represents front-side attack and **TS[3a-10a]/TS[3b-10b]** back-side attack.

As depicted in Table 1 and Figure 5, for the heavier hafnium congener the QR method affords geometries and relative energies that differ considerably from the simple FO approach. Thus, changes in density and geometry induced by relativity are important in the case of the heavier 5d elements.

The relativistic optimization reveals that the cationic alkyl hafnium complex **1c** favors a trigonal-pyramidal structure with the  $\alpha$ -carbon of the propyl group lying out of the nitrogen-hafnium-nitrogen plane, whereas the nonrelativistic structure is trigonal planar for hafnium (**1c'** of Figure 5). Trigonal-planar conformations are favored for the lighter zirconium, **1b**, and titanium, **1a**, analogues. The trigonal-planar coordina-

tion allows for the maximization of the  $\pi$ -donation from the lone-pair orbitals of the nitrogen to the empty  $d_\pi$  metal orbitals, whereas the trigonal-pyramidal geometry enhances the  $\sigma$ -interactions.<sup>51</sup> For the titanium and zirconium complexes, the empty  $d_\pi$  metal orbitals readily accept charge from the nitrogen lone pair orbitals and so the trigonal-planar coordination is favored. In the case of the hafnium system, the relativistic destabilization of d-orbitals<sup>52</sup> causes the  $d_\pi$  hafnium orbitals to become less suitable as electron acceptors and the hafnium cationic alkyl complex re-

(52) Ziegler, T.; Tschinke, V.; Baerends, E. J.; Snijders, J. G.; Ravenek, W. *J. Phys. Chem.* **1989**, *93*, 3050.

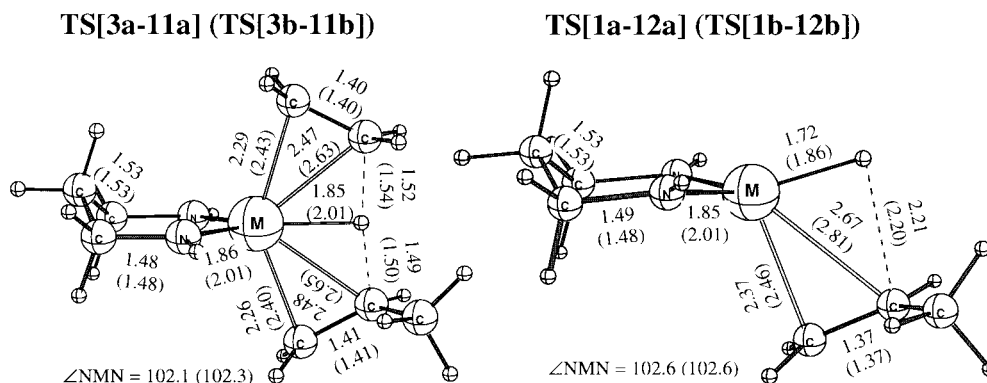


**Figure 4.** Optimization structures of the chain termination (transfer) transition states: **TS[3a-11a]/TS[3b-11b]** for the  $\beta$ -H transfer to the incoming ethylene, and **TS[1a-12a]/TS[1b-12b]** for the  $\beta$ -H elimination to the metal.

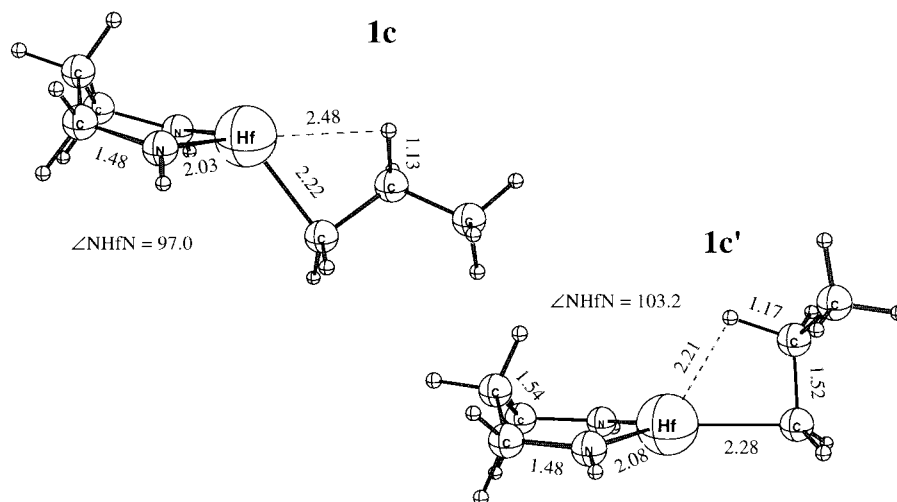


**Figure 5.** Comparison of the optimized geometries at the relativistic and nonrelativistic levels for the hafnium alkyl complex, *endo*-[HN(CH<sub>2</sub>)<sub>3</sub>NH]HfC<sub>3</sub>H<sub>7</sub><sup>+</sup>. The optimized geometry by the QR method is **1c**. The corresponding nonrelativistic geometry **1c'**.

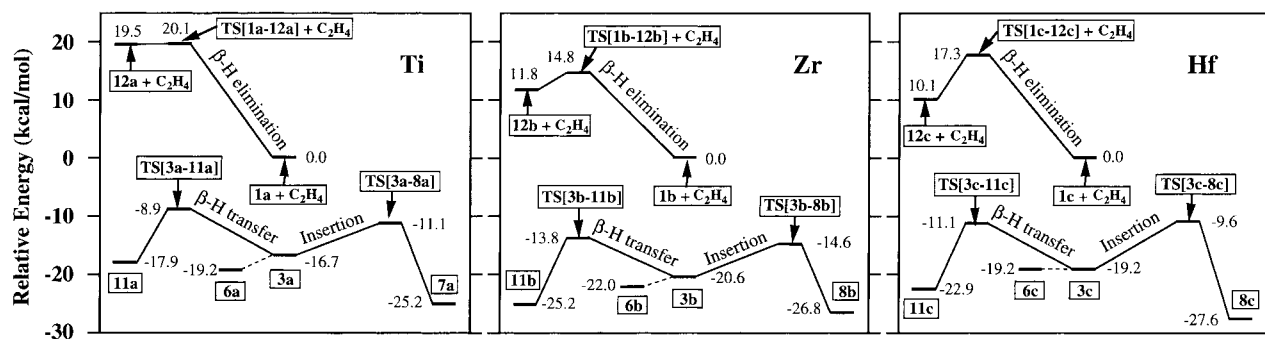


**Figure 6.** Comparison of the potential energy surfaces for the chain propagation and chain termination processes of the titanium, zirconium, and hafnium systems.

sorts to the trigonal-pyramidal structure which is preferred by the  $\sigma$ -framework.

**iii. Dependence of the Propagation and Termination Energy Profiles on the Metal Center.** Figure 6 depicts the energy profiles along the propagation and termination reaction paths for the generic group-4 systems. The catalytic cycle starts at the cationic endo-alkyl complexes (**1a/1b/1c**) by capturing an ethylene monomer to form the endo-FS  $\pi$ -complexes **3a/3b/3c**. The olefin complexation energies are 16.7 (**3a**), 20.6 (**3b**), and 19.2 kcal/mol (**3c**) for the Ti, Zr, and Hf systems, respectively. The trend in the ethylene uptake energy,

Zr > Hf  $\gg$  Ti, is found to be the same as for the bis-Cp metallocene systems of the group-4 elements.<sup>53</sup>

Starting from the  $\pi$ -complexes **3a/3b/3c**, the coordinated ethylene undergoes migratory insertion into the M-alkyl bond. The kinetic insertion barriers are 5.6 (Ti), 6.0 (Zr), and 9.6 kcal/mol (Hf). The hafnium system has a somewhat higher barrier since the framework for the cationic alkyl complex has to be deformed from the preferred trigonal-pyramidal conformation in the  $\pi$ -complex **3c** to the less favorable trigonal-planar geometry

(53) Yoshida, T.; Koga, N.; Morokuma, K. *Organometallics* **1995**, *14*, 746.



in the transition state TS[3c–8c]. For titanium and zirconium,<sup>51</sup> the  $\pi$ -complexes **3a/3b** already have the planar conformation in the transition states TS[3a–8a]/TS[3b–8b]. Thus, relativistic effects have a subtle but significant influence on trends in the barrier of insertion within the group-4 triad.

The kinetic product from the insertion are the  $\gamma$ -agostic metal–alkyl complexes (**8a/8b/8c**), and the exothermicities of the reaction are, respectively, –8.0 (Ti), –6.2 (Zr), and –8.4 kcal/mol (Hf). The titanium system, **8a**, can convert to the more stable  $\beta$ -agostic complex **7a**. On the other hand, for the zirconium and hafnium systems, the  $\gamma$ -agostic complexes turn out to be both the kinetic and thermodynamic products. The reason for this is that the larger radius of the heavier metal atoms allows a second  $\gamma$ -H interaction.

It follows from Figure 6 that the unimolecular  $\beta$ -H elimination channel is unfavorable from both a kinetic and thermodynamic point of view for all three metal atoms (this is true under normal monomer-rich polymerization conditions). The barriers are 20.1 (Ti), 14.8 (Zr), and 17.3 kcal/mol (Hf), respectively, and the endothermicities are 19.5 (Ti), 11.8 (Zr), and 10.1 kcal/mol (Hf).

On the other hand, the hydride transfer to the monomer (Scheme 2) chain termination channel seems to be operative. The overall barrier heights and endothermicities are, respectively, 10.3 and 1.3 kcal/mol, 8.2 and –3.2 kcal/mol, as well as 10.1 and –1.7 kcal/mol for M = Ti, Zr, and Hf, respectively.

It can be seen from Table 1 that the difference in barrier height between chain propagation and termination,  $\Delta E^\ddagger_{\text{termination}} - \Delta E^\ddagger_{\text{insertion}}$ , for the three metals is 2.2 (Ti), 0.8 (Zr), and –1.5 kcal/mol (Hf), respectively. This would indicate that for the generic systems both the titanium and zirconium diamide complexes are at best oligomerization catalysts whereas the hafnium analogue would hardly be able to act even as an ethylene dimerization catalyst. It is clear from our study of the generic titanium system that the bulky aryl substituents in the McConville diamide complex must play an important role in making it a living olefin polymerization catalyst. We shall now turn to a discussion of the bulky diamide complexes [ArNCH<sub>2</sub>CH<sub>2</sub>CH<sub>2</sub>–NAr]MR<sup>+</sup> with Ar = 2,6-<sup>i</sup>Pr<sub>2</sub>–C<sub>6</sub>H<sub>3</sub> and M = Ti, Zr.

**C. The Real Catalysts—Roles of the Ancillary Bulky Ligands. i. The Titanium System. Structures of Stationary Points.** We have considered all possible conformations of the cationic alkyl system [ArNCH<sub>2</sub>CH<sub>2</sub>CH<sub>2</sub>NAr]TiC<sub>3</sub>H<sub>7</sub><sup>+</sup> and the corresponding ethylene  $\pi$ -complex. In contrast to the generic system, the exo alkyl–titanium complex **2A** is found to be slightly more stable than the endo conformer **1A** by 0.6 kcal/mol. This can be understood by observing that in order to avoid steric repulsion between the isopropyl substituents and the propyl group (polymer chain), the two aryl rings tend to rotate away from the propyl group. In the case of **1A**, the rotation is somewhat hindered by the unique CH<sub>2</sub> group in the diamide ring. As a result, the steric repulsion (MM energies) is 1.2 kcal/mol higher in **1A** than that in **2A**. On the other hand, the electronic (QM) energy is 0.6 kcal/mol lower for **1A** compared to **2A**. The reason for **1A** being favored on electronic grounds is that the coordination center of

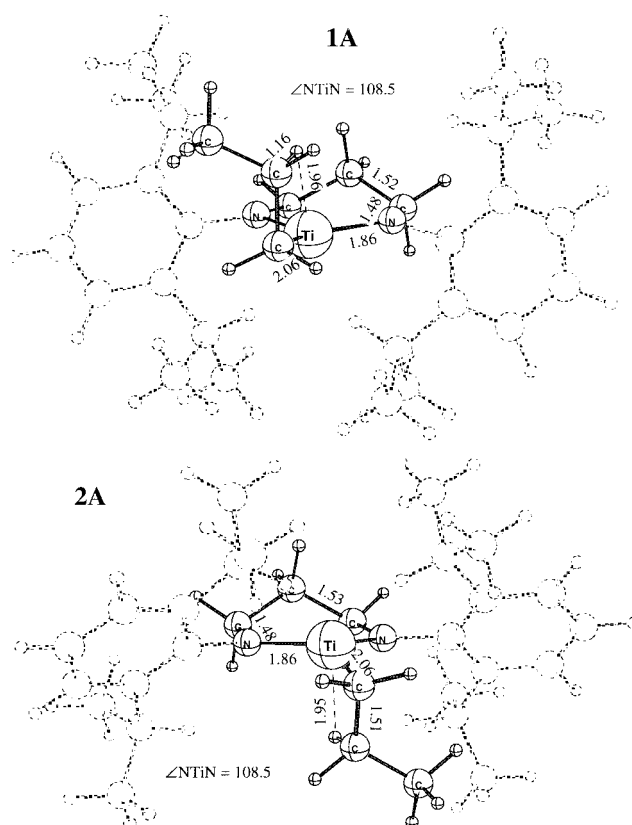


**Figure 7.** QM/MM-optimized structures for the McConville titanium complex.

**1A** is only slightly distorted from the optimal generic structure **1a**, whereas **2A** is considerably deformed from **2a**. We also notice from Figure 7 that the specific direction of the C(aryl)–N–N bending opens up the syn-side of the propyl group **1A** and **2A** while simultaneously closing the anti-side. We shall see in the next section that this will favor front-side attack of ethylene on both **1A** and **2A**.

The calculated relative energies shown in Figure 8 for the four different conformations of the Ti(IV)–alkyl ethylene  $\pi$ -complex follow the order: 0.0 (endo-FS, **3A**) < 2.0 (exo-BS, **6A**)  $\ll$  7.3 (exo-FS, **5A**) < 9.2 kcal/mol (**4A**, endo-BS). The energy decomposition analysis revealed that the order is governed by the steric interaction between the bulky aryl groups and the incoming ethylene. The endo-FS complex **3A** is the most stable since attack by ethylene from the syn-side of the propyl group in **1A** is unhindered. Therefore, in the following we shall base our discussion of the propagation and termination steps on the endo-FS  $\pi$ -complex.

The QM part of the insertion transition state (TS[**3A**–**8A**]) of Figure 9 is quite similar to the generic (TS[**3a**–**8a**]) structure. The most distinguishing feature is the formation of an  $\alpha$ -agostic bond as evidenced by the short Ti–H( $\alpha$ ) distance, 2.02 Å in TS[**3A**–**8A**] and 2.01 Å in TS[**3a**–**8a**]. On the other hand, the QM part of the TS for hydride transfer (TS[**3A**–**11A**]) differs considerably from its generic analogue, TS[**3a**–**11a**]. In particular, TS[**3A**–**11A**] is seen to be compressed along the axial positions by the isopropyl groups. Thus, the C( $\beta$ )–H( $\beta$ ) distance shrinks from 1.49 Å in TS[**3a**–**11a**] to 1.45 Å in TS[**3A**–**11A**]. It is evident from TS[**3A**–**11A**] that there is considerable steric interaction between the isopropyl substituents on the aryl groups with, respec-



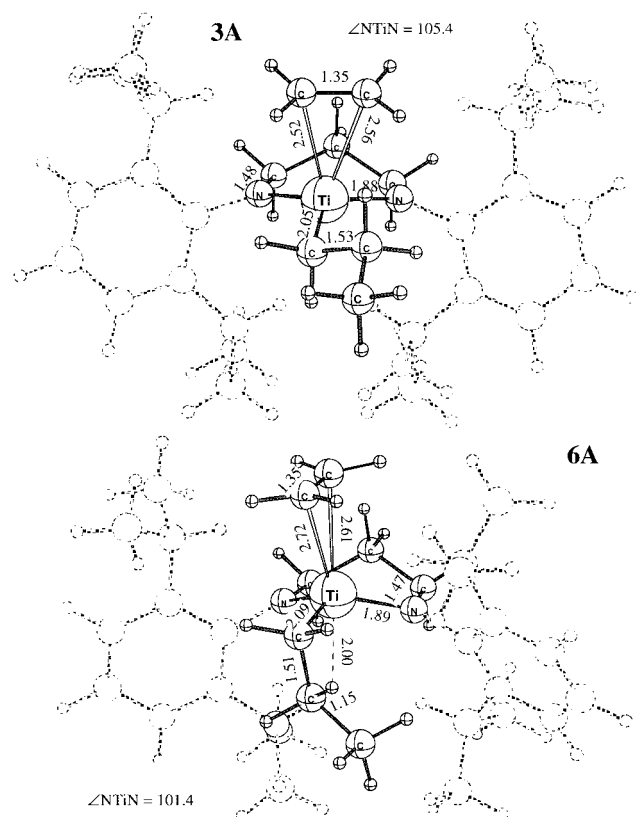


**Figure 8.** QM/MM-optimized structure of the most stable  $\pi$ -complex of the McConville titanium system.

tively, ethylene (monomer) and the propyl growing chain in the axial positions.

#### Potential Energy Surfaces of Titanium Systems.

Figure 10 compares the energy profiles along the propagation and termination reaction paths of the McConville catalyst with the generic titanium system. The catalytic cycle starts from the cationic titanium-alkyl complex (**1a/1A**) and a free ethylene monomer, middle of Figure 10. At the bottom of the figure, the catalyst (**1a/1A**) captures an incoming ethylene to form the resting states, **3a/3A**, with complexation energies of 16.7 and 17.0 kcal/mol for **3a** and **3A**, respectively. We note here that **3a** can readily convert to the more stable conformation **6a**, which we will label the ground-state  $\pi$ -complex for the unsubstituted system.

Starting from the ethylene  $\pi$ -complexes, **6a/3A**, to the right of Figure 10, the chain propagation commences by migratory insertion of the coordinated ethylene into the Ti-alkyl bond. The heats of reaction are found to be  $-6.0$  and  $-10.5$  kcal/mol, and the insertion barriers are 8.1 and 9.4 kcal/mol, for the generic and substituted titanium systems, respectively.

Also shown in Figure 10 are the energy profiles for the two chain termination channels. Plotted in the left lower part is the hydride transfer profile. The overall barrier and endothermicity for the generic system amounts to 10.3 and 1.3 kcal/mol, respectively. By taking the bulky substituents into account, we find that the barrier increases dramatically to 19.2 kcal/mol while the process becomes endothermic by 3.3 kcal/mol for the substituted system. Thus, the aryl groups are seen to retard this termination channel to a large extent both kinetically and thermodynamically. On the other hand, the bulky substituents only moderately alter the energy

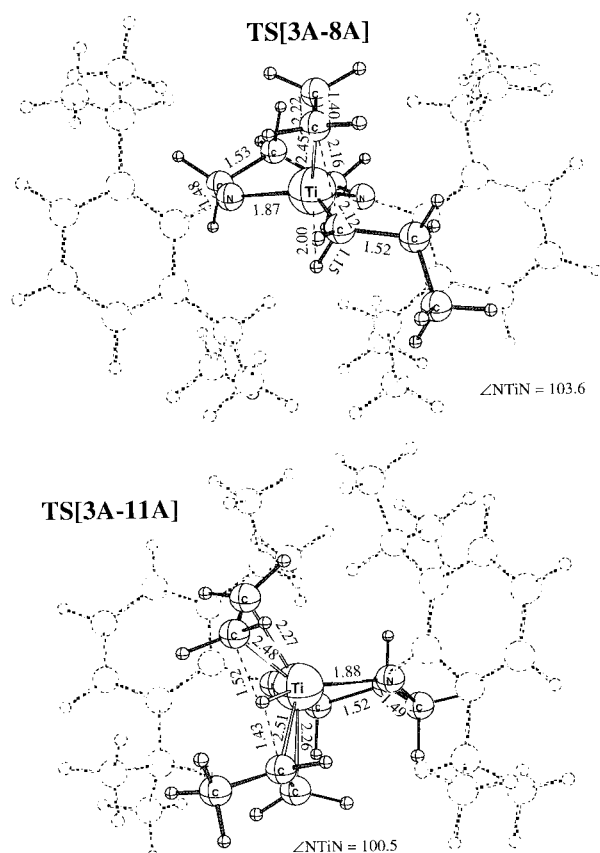


**Figure 9.** Comparison of the QM/MM-optimized transition states for chain propagation and termination of the McConville titanium system.

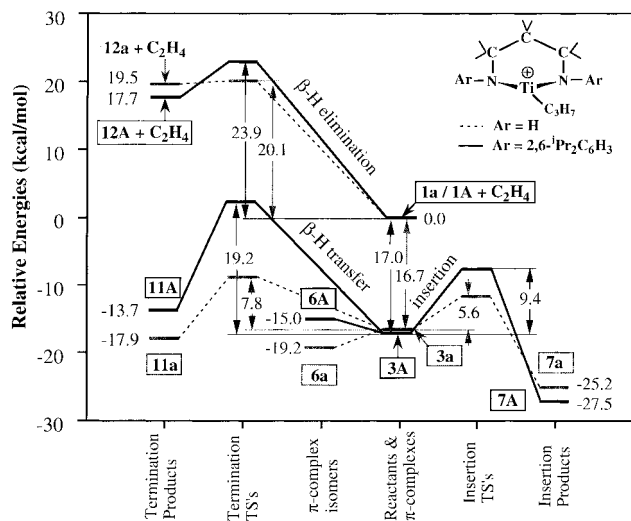


**Figure 10.** Comparison of the potential energy surfaces of the generic and substituted titanium systems.

profile for the chain termination path by  $\beta$ -H elimination (see left-upper part of Figure 10). Thus, the endothermicity of  $\beta$ -H elimination changes from 19.5 kcal/mol for the generic system to 17.7 kcal/mol for the substituted system and the corresponding barriers increase from 20.1 to 23.9 kcal/mol.

$\beta$ -H transfer is reversible, and the coordinated vinyl-terminated chain can "re-insert". This can lead to further propagation unless the vinyl-terminated polymer chain can be displaced from the metal by ethylene. One might argue that this displacement process is the

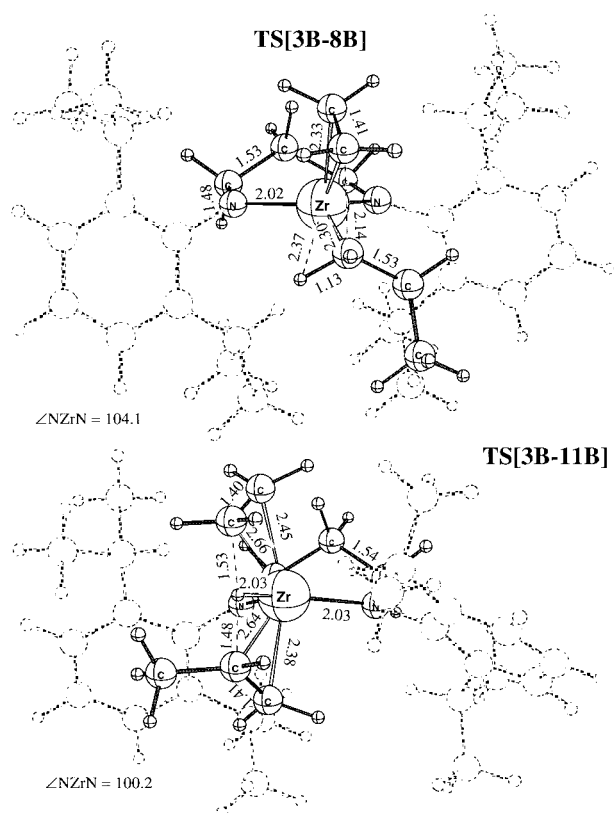


**Figure 11.** Comparison of the insertion and termination transition states for the McConville zirconium systems.

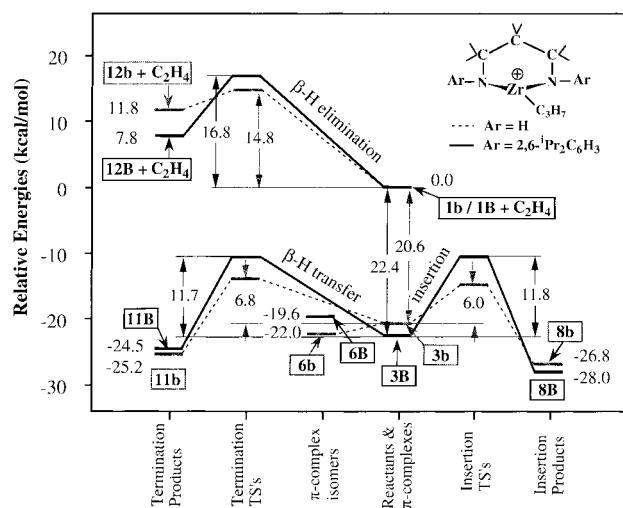


**Figure 12.** Comparison of the potential energy surfaces for the generic and substituted zirconium systems.

real rate-determining step of the overall termination. The enthalpic cost for the unimolecular dissociation is due to the loss of the complexation energy between the vinyl-terminated polymer chain and the metal, which can be estimated from the calculated ethylene complexation energy to be between 17 and 22 kcal/mol (Figures 10 and 12). However, these values do not include zero-point energy (ZPE) and  $T\Delta S$  contributions. It is our experience that the ZPE contribution to chain ejection is about 3–4 kcal/mol. From both calculations<sup>51</sup> and experiment,<sup>62</sup> it is known that the  $T\Delta S$  contribution at 300 K for the ethylene ejection process is about 10 kcal/mol. If one subtracts these values from the above-mentioned endothermicities, one arrives at an estimate

of ca. 3 and 8 kcal/mol for the ejection free energy for the titanium and zirconium systems, respectively. This is not enough for the ejection process to become the rate-determining step for the termination of the real systems. Only for the generic zirconium system may the chain ejection barrier be comparable with the hydrogen transfer barrier.

In summary, the bulky aryl substituents act to enhance the exothermicity of the chain propagation step by 4.5 kcal/mol and increase the endothermicity of the chain termination step by 2.0 kcal/mol. More importantly, the aryl groups increase the difference in the barrier heights between chain propagation and chain termination,  $\Delta E_{\text{termination}}^{\ddagger} - \Delta E_{\text{insertion}}^{\ddagger}$ , from 2.2 to 9.8 kcal/mol. Thus, the bulky substituents are a necessary component in making the McConville diamide titanium complex a living catalyst for polymerization of  $\alpha$ -olefins.

**ii. The Zirconium System.** The endo-FS conformation, **3B** of Figure 11, is also found to be the preferred geometry for the zirconium ethylene complex. The exo-BS  $\pi$ -complex, **6B**, is higher in energy by 2.8 kcal/mol. Hence, the dominant propagation path starts from ethylene uptake of **1B** to form **3B**, followed by insertion of the coordinated ethylene into the Zr–alkyl bond to form the new alkyl species **8B** via the transition state TS[**3B**–**8B**]. The competing chain termination process transfers a  $\beta$ -hydrogen on the propyl growing chain to the ethylene monomer in **3B** through the TS[**3B**–**11B**] transition state. The result is a Zr–ethyl propene  $\pi$ -complex, **11B**. Figure 12 summarizes the energetics for the catalytic processes of the zirconium systems.

It can be seen from Figure 12 that the ethylene uptake energies, –20.6 (**3b**) and –22.0 kcal/mol (**6b**) for the generic system, are similar to the uptake energy of 22.4 kcal/mol for the substituted system (**3B**). For the chain propagation (the right side of Figure 12), the overall insertion barrier increases from 7.4 kcal/mol for the generic system, TS[**3b**–**8b**] to 11.8 kcal/mol for the substituted system, TS[**3B**–**8B**]. At the same time, the exothermicity of the insertion reaction changes slightly from 4.8 kcal/mol in the generic system, **8b**, to 5.6 kcal/mol for the substituted system, **8B**.

For the chain termination channels (the left side of Figure 12), the bulky substituents increase the activation barriers by 3.5 and 2.0 kcal/mol for  $\beta$ -H transfer (lower-right profile of Figure 12) and  $\beta$ -H elimination (upper-right of Figure 12), respectively. Meanwhile, the bulky substituents destabilize the  $\beta$ -H transfer chain termination products **11B** by 1.1 kcal/mol and stabilize the  $\beta$ -H elimination product **12B** by 4.0 kcal/mol. Figure 12 further shows that the index for the polymerization ability of the Zr catalysts,  $\Delta E_{\text{termination}}^{\ddagger} - \Delta E_{\text{insertion}}^{\ddagger}$ , drops from 0.8 to –0.1 kcal/mol as the aryl substituents are added. Overall, Figure 12 illustrates that the energy profiles for the zirconium systems with and without bulky substituents are qualitatively the same. Thus, the steric bulk which in the titanium case was able to turn the generic system into a living catalyst is unable to do so in the zirconium case.

By analyzing the structures of the stationary points along the reaction path and comparing them to the titanium systems, we find that the decisive factor accounting for the drastically different catalytic behavior of the McConville-type titanium and zirconium

**Table 2. Relative Energies for the McConville-Type Titanium and Zirconium Diamide Catalytic Systems<sup>a</sup>**

species <sup>b</sup>	Ti			Zr		
	QM	MM	total	QM	MM	total
<b>3A/3B</b>	0.0	0.0	0.0	0.0	0.0	0.0
<b>1A/1B</b> + C <sub>2</sub> H <sub>4</sub>	17.1	-0.1	17.0	20.4	2.0	22.4
<b>TS[3A-8A]/[3B-8B]</b>	5.2	4.2	9.4	8.3	3.5	11.8
<b>TS[3A-11A]/[3B-11B]</b>	11.4	7.8	19.2	8.5	3.2	11.7
<b>7A/8B</b>	-7.5	-3.0	-10.5	-6.0	0.4	-5.6
<b>11A/11B</b>	-0.7	4.0	3.3	-3.0	0.9	-2.1

<sup>a</sup> Energies in kcal/mol, relative to **3A** and **3B** for the titanium and zirconium systems, respectively. <sup>b</sup> **3A/3B**: the metal-alkyl ethylene  $\pi$ -complexes. **1A/1B**: the metal-alkyl complexes, the active catalysts. **TS[3A-8A]/[3B-8B]**: the insertion transition states. **TS[3A-11A]/[3B-11B]**: the  $\beta$ -H transfer (the chain termination) transition states. **7A/8B**: the thermodynamic products of the insertion. **11A/11B**: the chain termination products.

diamide complexes is the different sizes of the metals, Figure 11. The larger radius of zirconium increases the M-N bond distance, which makes it possible for the aryl rings to move away from the position perpendicular to the N-Zr-N plane without substantial steric interaction between the isopropyl groups and the (CH<sub>2</sub>)<sub>3</sub> diamide bridge. When the aryl rings are perpendicular to one another, the isopropyl groups are unable to retard the chain termination process since they no longer block the axial sites. Thus, whereas TS[**3A-11A**] of the titanium system is seen to be destabilized by 7.8 kcal/mol from steric interactions (Table 2), the MM contribution to TS[**3B-11B**] is seen to be negligible.

**D. Comparison of Theoretical and Experimental Results. Structures.** Scollard and McConville have structurally characterized the chelating diamide complexes of titanium and zirconium: [ArN(CH<sub>2</sub>)<sub>3</sub>NAr]-TiCl<sub>2</sub><sup>+</sup>,<sup>7</sup> [ArN(CH<sub>2</sub>)<sub>3</sub>NAr]Ti[CH<sub>2</sub>B(C<sub>6</sub>F<sub>5</sub>)<sub>2</sub>](C<sub>6</sub>F<sub>5</sub>),<sup>45</sup> and [ArN(CH<sub>2</sub>)<sub>3</sub>NAr]Zr( $\eta^2$ (N,C)-NC<sub>5</sub>H<sub>4</sub>)(CH<sub>2</sub>CMe<sub>2</sub>Ph)<sup>54</sup> with Ar = 2,6-<sup>i</sup>Pr<sub>2</sub>-C<sub>6</sub>H<sub>3</sub>, as well as [ArN(CH<sub>2</sub>)<sub>3</sub>NAr]TiMe<sub>2</sub><sup>+</sup><sup>54</sup> with Ar = 2,6-Me<sub>2</sub>-C<sub>6</sub>H<sub>3</sub>. They demonstrated that all the complexes could be described as a distorted tetrahedron with the aryl groups situated perpendicular to the N-Ti-N plane. Their structural data also showed that the two C(aryl)-N bonds as well as the (CH<sub>2</sub>)<sub>3</sub> diamide bridge flip out of the N-M-N (M = Ti, Zr) plane. Cloke et al.<sup>55</sup> have characterized the benzyl-substituted chelating diamide ligated zirconium complex [ArDABP]Zr(CH<sub>2</sub>Ph)<sub>2</sub> (ArDABP = 2,2'-di(*N*-benzyl)-amino-6,6'-dimethylbiphenyl, Ar = CH<sub>2</sub>C<sub>6</sub>H<sub>4</sub>Ph-4). Our optimized QM/MM structures for all four-coordinated metal-alkyl ethylene complexes reproduce the experimental trends for the aryl rings and the diamide bridge. Further, the experiments determined that the Ti-N and Ti-C(alkyl) bond lengths range, respectively, from 1.839 to 1.867 Å and from 2.077 to 2.191 Å. Also, the N-Ti-N angle lies in the range from 99.2° to 102.6°. The theoretical values for the five structures (**3A-6A**, **11A**) are, respectively, 1.865-1.888 Å for the Ti-N bonds, 2.066-2.10 Å for the Ti-C(alkyl) bonds, and 98.4-105.4° for the N-Ti-N angles. For the four-coordinated Zr diamide complexes, the experimental values are 2.031-2.071 Å (Zr-N), 2.260-2.296 Å [Zr-C(alkyl)],

and 95.4-109.35° (N-Zr-N). The corresponding theoretical values for **3B**, **6B**, and **11B** are 2.019-2.038 Å, 2.218-2.257 Å, and 100.2-101.2°, respectively. The comparison given above suggests that the QM/MM-optimized geometries for the diamide complexes of group-4 metals are in good agreement with the experimental structures.

**Energetics and Catalytic Activities.** In their series of studies, Scollard and McConville have demonstrated that the cationic chelating diamide complexes of titanium [ArN(CH<sub>2</sub>)<sub>3</sub>NAr]Ti(IV)CH<sub>3</sub><sup>+</sup> (Ar = 2,6-<sup>i</sup>Pr<sub>2</sub>C<sub>6</sub>H<sub>3</sub>, 2,6-Me<sub>2</sub>C<sub>6</sub>H<sub>3</sub>) serve as effective catalysts for the living polymerization of  $\alpha$ -olefin.<sup>6,7,45</sup> Our study has shown that the energetically most favorable chain termination channel is  $\beta$ -H transfer to the incoming monomer. The calculated energy barrier for this path is 19.2 kcal/mol, which is 9.8 kcal/mol higher than the barrier of chain propagation from the same ethylene complex **3A**. The weight-average molecular weight,  $M_w$ , can be estimated<sup>13</sup> from this value to be  $4.8 \times 10^8$  g/mol, implying that the catalyst can perform living polymerization of ethylene. Experiments<sup>56</sup> indicate that the analogous catalyst of zirconium could only serve to oligomerize  $\alpha$ -olefins with  $n = 2-7$ . In line with the experimental results, the calculations found the difference in barrier height between the insertion and termination processes to be 0.1 kcal/mol for the substituted zirconium system. This would imply that the zirconium diamide complex [ArN(CH<sub>2</sub>)<sub>3</sub>NAr]Zr(VI)CH<sub>3</sub><sup>+</sup> (Ar = 2,6-<sup>i</sup>Pr<sub>2</sub>C<sub>6</sub>H<sub>3</sub>) in average could serve as an ethylene dimerization catalyst. Thus, we conclude that for the larger zirconium atom, even bulkier groups have to be employed in order to generate an efficient catalyst.

The idea that bulkier ligands might improve the polymerization capability of the zirconium catalyst can be deduced from several recent investigations. For instance, the Schrock group<sup>8</sup> has reported that activated tridentate diamide complexes of zirconium [((*t*-Bu-*d*<sub>6</sub>)N-*o*-C<sub>6</sub>H<sub>4</sub>)<sub>2</sub>O]ZrMe<sub>2</sub> polymerize 1-hexene and ethylene efficiently. The X-ray structural data showed that at least one axial position of the activated species would be blocked by a CH<sub>3</sub>-group of the *tert*-butyl substituent on nitrogen. Horton et al.<sup>57</sup> synthesized and characterized the zirconium tridentate diamide complexes [Me<sub>3</sub>-SiN(CH<sub>2</sub>CH<sub>2</sub>NSiMe<sub>3</sub>)<sub>2</sub>]ZrR<sub>2</sub> (N<sub>3</sub>ZrR<sub>2</sub>; R = CH<sub>2</sub>Ph, Me) in which the two diamide nitrogens lie on the equatorial plane while the bridging nitrogen is occupying an axial position. They found that the activated diamide complexes N<sub>3</sub>ZrR<sub>2</sub> produced high molecular weight polyethylene. Cloke and co-workers<sup>55</sup> found that the zirconium diamide complexes [(C<sub>6</sub>H<sub>3</sub>)<sub>2</sub>-2,2'-(NCH<sub>2</sub>C<sub>6</sub>H<sub>4</sub>Ph-4)-2,6,6'-Me<sub>2</sub>]Zr( $\eta^1$ -CH<sub>2</sub>Ph)( $\eta^2$ -CH<sub>2</sub>Ph) activated by MAO are capable of polymerizing ethylene. The crystal structures reveal that the two C<sub>6</sub>H<sub>4</sub>R-4 groups attached to nitrogen will block the axial sites. We believe that the large volume of ancillary ligands in the Cloke complexes also destabilizes the  $\pi$ -complexes and the insertion TS's as well, resulting in polyethylene with relatively low  $M_w$ .

Compared to the novel zirconium diamide complexes mentioned above, the McConville-type diamide complexes with aryl rings directly linked to the chelating

(54) Scollard, J. D.; McConville, D. H.; Vittal, J. J. *Organometallics* **1995**, *14*, 5478.

(55) Cloke, F. G. N.; Geldbach, T. J. G.; Hitchcock, P. B.; Love, J. J. *Organomet. Chem.* **1996**, *506*, 343.

(56) McConville, D. H. Department Chemistry, University of British Columbia, private communication.

(57) Horton, A. D.; de With, J.; van der Linden, A. J.; van de Weg, H. *Organometallics* **1996**, *15*, 2672.



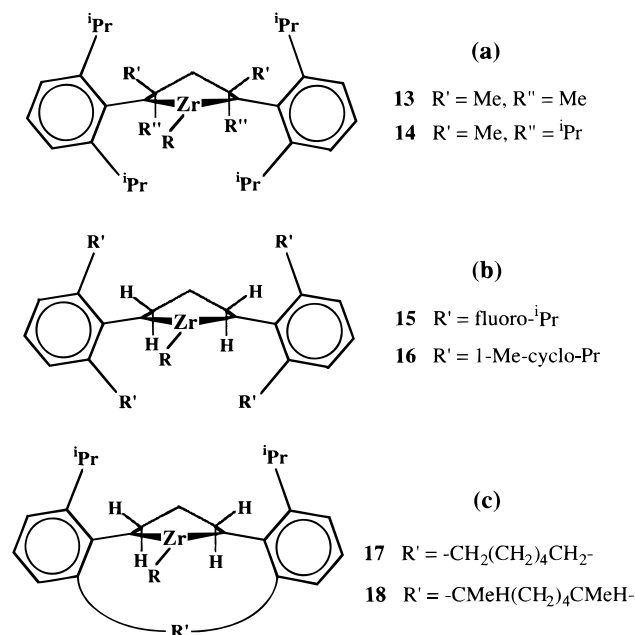


**Figure 13.** Structures for the designed new catalysts.

nitrogen atoms have several advantages. In the first place, adding bulky substituents to the planar two-dimensional aryl rings suppresses exclusively the termination step by shielding the space above and below the N–M–N plane in the axial direction. On the other hand, space is left in the equatorial plane for the propagation to proceed unencumbered. Further, the tilt of the  $(\text{CH}_2)_3$  diamide bridge out of the equatorial N–M–N plane opens the prospect for stereoregular olefin polymerization.

**E. Design of New Catalysts on the Basis of the Zirconium Diamide Complexes.** On the basis of the criterion established by the previous discussion, we propose three types of ligand modifications to improve the polymerization capability of the zirconium diamide complexes. Figure 13 illustrates the structures of the proposed catalysts. Molecular modeling using the QM/MM method has been carried out for the ethylene polymerization by these new catalysts. Fully optimized geometries of the Zr(IV)–alkyl complexes, Zr–alkyl ethylene  $\pi$ -complexes, and the chain propagation and chain transfer transition states are provided in the Supporting Information. Table 3 summarizes the energetics for the elementary reaction steps based on the three proposed catalysts together with the calculated weight-average molecular weight,  $M_w$ . The corresponding theoretical and experimental results for the Brookhart-type Ni(II)–diimide system as well as the original McConville systems are also compiled in Table 3 for comparison.

Essentially, any improvement must prevent the aryl rings from moving away from the position perpendicular to the N–Zr–N plane since such a movement exposes the axial position to termination by  $\beta$ -H transfer. We shall now discuss three strategies that will increase the activation barrier for the chain termination step in the zirconium-based diamides.

**Increasing the Steric Bulk on the Diamide Bridge.** Increasing the bulk of the diamide alkyl bridge by substituting the hydrogens with methyl groups should generate sufficient steric interaction with the

isopropyl groups to prevent the aryl rings from rotating even with the longer Zr–N bonds. In complex **13**, the carbons in the amide bridge closest to nitrogen carry methyl groups. The calculated values of 2.8 kcal/mol and 3300 g/mol for  $\Delta E^\ddagger_{\text{termination}} - \Delta E^\ddagger_{\text{insertion}}$  and  $M_w$  (Table 3) indicate that the simple modification enhances the polymerization ability of McConville's zirconium diamide complex significantly. The  $M_w$  of polyethylene produced by **13** is, thus, comparable to that of the  $[(\text{C}_6\text{H}_3)_2-2,2',2''\text{-(NCH}_2\text{C}_6\text{H}_4\text{Ph-4)}_2\text{-6,6'-Me}_2]\text{Zr}(\eta^1\text{-CH}_2\text{Ph})\text{-(}\eta^2\text{-CH}_2\text{Ph)}$  olefin polymerization catalyst of Horton et al.<sup>57</sup> Considering the fact that the catalytic center of **13** is much more open in the equatorial plane than Horton's catalysts, we predict that complex **13** has a higher activity for ethylene polymerization.

Increasing the bulk of the diamide bridge in **13** by replacing the two methyl groups exo to the incoming monomer with  $i\text{Pr}$  substituents,  $R''$  of Figure 13a, results in the improved catalyst **14**. For **14**, the calculated  $\Delta E^\ddagger_{\text{termination}} - \Delta E^\ddagger_{\text{insertion}}$  is 3.8 kcal/mol, giving a calculated  $M_w$  of 18 000 g/mol. These results suggest that the catalyst should produce polymers of similar  $M_w$  to that of Schrock's catalyst<sup>8</sup> for ethylene polymerization. Additionally, the low insertion barrier of 2.9 kcal/mol is likely to make **14** more active. An attempt to further increase the steric bulk of the diamide bridge did not increase the catalytic performance. Instead, ethylene is eventually prevented from coordinating to the metal center.

**Increasing Steric Bulk on the Aryl Rings.** It might be possible to keep the aryl groups in their upright perpendicular position by increasing the steric bulk on the isopropyl groups rather than the diamide bridge. Complex **15** (Figure 12b) represents a possible candidate in which isopropyl is replaced by fluoro- $i\text{Pr}$  groups. QM/MM calculations on the termination transition state of **15** reveal that the aryl rings are in a perpendicular position with respect to the N–Zr–N plane. As a consequence, the steric repulsion between the F- $i\text{Pr}$  groups and ethylene (above the N–Zr–N plane) as well as between the F- $i\text{Pr}$  groups and the growing chain (below the N–Zr–N plane) are substantial. Thus the  $\Delta E^\ddagger_{\text{termination}} - \Delta E^\ddagger_{\text{insertion}}$  value increases from  $-0.1$  kcal/mol in the original system **1B** to 7.1 kcal/mol for the modified system **15**.

As a further advantage, the insertion barrier in **15** of 2.1 kcal/mol has decreased drastically compared to **1B** for which the insertion barrier was 11.1 kcal/mol, Table 3. The increase in activity comes from a destabilization of the Zr(IV)–alkyl ethylene  $\pi$ -complex as a result of steric repulsion between ethylene and the bulkier F- $i\text{Pr}$  groups. Thus, the ethylene complexation energy is seen to be reduced from 22.2 to 13.2 kcal/mol, Table 3. Our calculations would suggest that **15** would provide living polymerization characteristics similar to that of the original titanium complex **1A** by McConville. However, the suggested zirconium system **15** would have a much higher activity due to the low insertion barrier.

As an alternative to F- $i\text{Pr}$ , Piers<sup>58</sup> suggested the use 1-Me-cyclopropyl (**16**, Figure 12b), which is similar in steric bulk to F- $i\text{Pr}$ . The optimized structures show that both aryl rings are perpendicular to the N–Zr–N plane

(58) Piers, W. Department Chemistry, The University of Calgary, private communication.

**Table 3. Comparison of the Catalytic Ability of the New Catalysts with the McConville and Brookhart Catalysts for Polymerization of Ethylene**

catalysts	$\Delta E_{\text{uptake}}^a$	$\Delta E_{\text{insertion}}^a$	$\Delta(\Delta E^\ddagger)^a$	$M_w^b$
[ArN(CH <sub>2</sub> ) <sub>3</sub> NAr]MR <sup>+</sup> <sup>c</sup>				
M = Ti, Ar = 2,6- <sup>i</sup> Pr <sub>2</sub> C <sub>6</sub> H <sub>3</sub> ( <b>1A</b> )	17.0	9.4	9.9	5.6 × 10 <sup>8</sup> (living)
M = Zr, Ar = 2,6- <sup>i</sup> Pr <sub>2</sub> C <sub>6</sub> H <sub>3</sub> ( <b>1B</b> )	22.4	11.8	-0.1	dimmer (2-7)
[ArNCR''R'CH <sub>2</sub> CR'R''NAr]ZrR <sup>+</sup>				
R' = R'' = CH <sub>3</sub> ( <b>13</b> )	22.3	9.2	2.8	3.3 × 10 <sup>3</sup>
R' = CH <sub>3</sub> , R'' = <sup>i</sup> Pr ( <b>14</b> )	13.8	2.9	3.8	1.8 × 10 <sup>4</sup>
[ArN(CH <sub>2</sub> ) <sub>3</sub> NAr]ZrR <sup>+</sup>				
Ar = 2,6-(CMe <sub>2</sub> F) <sub>2</sub> -C <sub>6</sub> H <sub>3</sub> ( <b>15</b> )	13.2	2.1	7.1	4.9 × 10 <sup>6</sup>
Ar = 2,6-(1-Me- <i>cyclo</i> -Pr) <sub>2</sub> -C <sub>6</sub> H <sub>3</sub> ( <b>16</b> )	17.6	-1.7	8.9	1.0 × 10 <sup>8</sup>
[ArN(CH <sub>2</sub> ) <sub>3</sub> NAr]ZrR <sup>+</sup> (Ar = 1- <sup>i</sup> Pr, 6-R'-C <sub>6</sub> H <sub>3</sub> )				
R' = -CH <sub>2</sub> (CH <sub>2</sub> ) <sub>4</sub> CH <sub>2</sub> - ( <b>17</b> )	18.7	8.2	1.8	6.0 × 10 <sup>2</sup>
R' = -CHMe(CH <sub>2</sub> ) <sub>4</sub> CHMe- ( <b>18</b> )	17.9	3.3	8.6	6.2 × 10 <sup>7</sup>
[ArNCH <sub>2</sub> CH <sub>2</sub> NAr]NiR <sup>+</sup> <sup>d</sup>				
Ar = 2,6-( <sup>i</sup> Pr) <sub>2</sub> C <sub>6</sub> H <sub>3</sub>	14.9	13.2 (10-11)	5.4 (5.6)	5.8 × 10 <sup>4</sup> (8.1 × 10 <sup>4</sup> )

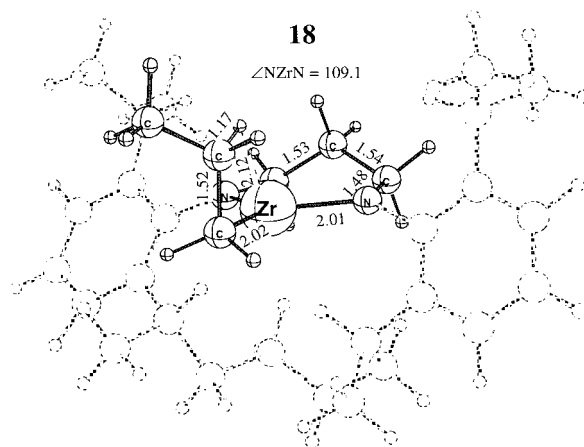
<sup>a</sup> Relative energies in kcal/mol.  $\Delta E_{\text{uptake}}$ : ethylene uptake energy.  $\Delta E_{\text{insertion}}^\ddagger$ : insertion barrier.  $\Delta(\Delta E^\ddagger)$ : the difference in activation energy between insertion (chain propagation) and termination. Experimental values in parentheses. <sup>b</sup> Weight-average molecular weight,  $M_w$ , estimated from the  $\Delta(\Delta E^\ddagger)$  values using Boltzmann statistics at 296.15 K for the diamide systems, and at 298.15 K for the Brookhart system. In parentheses are the experimental results; for **1B** the experimental result is expressed as the monomer contained in the product.

<sup>c</sup> The McConville catalysts, ref 6 and private communication from Prof. McConville. Monomer used in the experiments are 1-hexene. <sup>d</sup> The Brookhart catalysts, ref 11 for the experimental results and ref 13 for the theoretical results. The experimental value of  $\Delta(\Delta G^\ddagger)$  estimated from the  $M_w$  in ref 11.

at the chain termination TS, TS[**16**-termination]. The calculated MM energy of TS[**16**-termination] relative to TS[**16**-insertion] is found to be 8.9 kcal/mol, which is nearly the same as the energy gap between the two TS's:  $\Delta E_{\text{termination}}^\ddagger - \Delta E_{\text{insertion}}^\ddagger = 8.9$  kcal/mol. For the system suggested by Piers, no barrier to insertion was found. It follows from Table 3 that  $\Delta E_{\text{uptake}}$  and  $\Delta E_{\text{termination}}^\ddagger - \Delta E_{\text{insertion}}^\ddagger$  for **16** are similar in magnitude to the corresponding terms of the McConville's Ti-diamide system, **1A**. This would suggest that **16** should also be a living ethylene polymerization catalyst, again with a higher activity than **1A**.

**Blocking One Axial Position by a Hydrocarbon Bridge.** Our last catalyst modification simply blocks off one axial position by a -CH<sub>2</sub>(CH<sub>2</sub>)<sub>4</sub>CH<sub>2</sub>- bridge connecting the two aryl rings as shown in **17**. With this modification, an ethylene monomer can still enter to form a  $\pi$ -complex and undergo insertion. However, the termination TS with two axial sites occupied should suffer considerable steric repulsion.

Comparing the relative energies for the proposed catalyst **17**, Table 3, with those of the McConville zirconium diamide system **1B** (Table 3 and Figure 11) and the corresponding generic system **1b** (Table 2 and Figure 6) indicates a modest improvement in the catalytic activity to a  $M_w$  value for polyethylene of 600 g/mol (Table 3). An MM energy decomposition analysis, also shown in Table 3, suggests that the bridge is still not restrictive enough to prevent the termination and increase the activity by destabilizing the  $\pi$ -complex. We, therefore, select the bridge -CHMe(CH<sub>2</sub>)<sub>4</sub>CHMe- that has one methyl group at each of the two carbons anchored directly to the aryl groups, **18** (Figure 13c). The QM/MM calculations for this system exhibit promising properties toward ethylene polymerization. Now,  $\Delta E_{\text{termination}}^\ddagger - \Delta E_{\text{insertion}}^\ddagger$  is 8.6 kcal/mol and the ethylene uptake energy becomes 17.9 kcal/mol, Table 3. These values are close to those of the living titanium polymerization catalyst, but **18** has a higher activity with an insertion barrier of only 3.3 kcal/mol.

**Figure 14.** QM/MM-optimized structure of the new bridged catalyst.

It follows from the structures related to **18**, Figure 14, that the catalyst is sufficiently rigid to allow for stereoregular olefin polymerization with appropriate substitutions.<sup>59-61</sup> This point will be explored further in a later study. It should also be possible to increase the  $\Delta E_{\text{termination}}^\ddagger - \Delta E_{\text{insertion}}^\ddagger$  value and allow for optimal copolymerization with  $\alpha$ -olefins by modifications of the bridge.

**Other Ligand Modifications.** The above-developed strategies open many possibilities in which one could retard chain termination and increase activity by destabilizing the  $\pi$ -complex. All would be based on the same principles in which the axial positions above and below the N-M-N plane are blocked by steric bulk. It

(59) Kaminsky, W.; Hulper, K.; Brintzinger, H. H.; Wild, F. *Angew. Chem., Int. Ed. Engl.* **1985**, *24*, 507.

(60) Schnutenhaus, H.; Brintzinger, H. H. *Angew. Chem., Int. Ed. Engl.* **1989**, *18*, 777.

(61) Huttenloch, M. E.; Diebold, J.; Rief, U.; Brintzinger, H. H.; Gilbert, A. M.; Katz, T. J. *Organometallics* **1992**, *11*, 3600.

(62) Rix, F. C.; Brookhart, M.; White, P. S. *J. Am. Chem. Soc.* **1996**, *118*, 4746.

(63) Bernardi, F.; Bottoni, A.; Calcinari, M.; Rossi, I.; Robb, M. A. *J. Phys. Chem. A* **1997**, *101*, 6310.

should even be possible to design ligands that would afford living olefin polymerization catalysts based on hafnium diamide complexes.

#### IV. Summary

We have applied pure quantum mechanical methods (DFT) as well as a combination of molecular mechanics and quantum mechanics (QM/MM) in an extensive study of ethylene polymerization by group-4 diamide complexes following the pioneering experimental work by McConville et al.<sup>6</sup>

The pure DFT study was confined to generic models with hydrogens attached to the chelating nitrogen atoms in place of the aryl rings used by McConville et al. in their experimental work. Modeling of the generic  $[\text{HNCH}_2\text{CH}_2\text{CH}_2\text{NH}]\text{MC}_3\text{H}_7^+$  systems reveals that the titanium, **1a**, and zirconium, **1b**, diamide complexes at most are oligomerization catalysts whereas the hafnium analogue, **1c**, is hardly able even to dimerize ethylene.

The quantitative results for the individual steps involving the reaction of ethylene with the generic  $[\text{HNCH}_2\text{CH}_2\text{CH}_2\text{NH}]\text{MC}_3\text{H}_7^+$  systems are (i) the ethylene complexation energies follow the order  $\text{Ti}$  (19.2 kcal/mol) <  $\text{Hf}$  (21.9 kcal/mol)  $\leq$   $\text{Zr}$  (22.0 kcal/mol); (ii) the overall insertion barriers (relative to the most stable  $\pi$ -complex) are  $\text{Zr}$  (7.4 kcal/mol)  $\leq$   $\text{Ti}$  (8.1 kcal/mol) <  $\text{Hf}$  (9.6 kcal/mol); and (iii) the chain termination barriers are  $\text{Hf}$  (8.1 kcal/mol)  $\approx$   $\text{Zr}$  (8.2 kcal/mol) <  $\text{Ti}$  (10.3 kcal/mol). The  $\beta$ -hydrogen transfer from the alkyl to the coordinated ethylene is found to be the operative chain termination channel. The corresponding unimolecular chain termination channel via  $\beta$ -hydrogen elimination to the metal center has a much higher barrier, following the order  $\text{Zr}$  (14.8 kcal/mol) <  $\text{Hf}$  (17.3 kcal/mol) <  $\text{Ti}$  (20.1 kcal/mol). The insertion transition state is stabilized by donation of charge from the nitrogen lone pairs into empty d-orbitals on the metal. For hafnium, relativistic effects increase the insertion barrier by destabilizing the d-orbitals and thus the insertion transition state.

The combined QM/MM method was applied to the real McConville catalyst  $[\text{ArN}(\text{CH}_2)_3\text{NAr}]\text{MR}^+$  ( $\text{M} = \text{Ti}, \text{Zr}$ ;  $\text{Ar} = 2,6\text{-}^i\text{Pr}_2\text{-C}_6\text{H}_3$ ) with aryl rings attached to the chelating nitrogens. We calculate the barrier of termination to be 9.8 kcal/mol higher than the barrier of propagation for the titanium system. On the other hand, the difference in activation energy between propagation and termination is 0.1 kcal/mol for the zirconium complex. Our results are in line with the findings by McConville that the titanium complex is a living olefin polymerization catalyst whereas the homologous zirconium complex only is able to oligomerize

olefins. An analysis of the results showed that the isopropyl-substituted aryl rings in the titanium system are forced to stay perpendicular to the  $\text{N-M-N}$  plane in order to avoid the steric bulk of the diamide bridge. In this orientation, the axial sites above and below the  $\text{N-Ti-N}$  plane are blocked and the termination transition state destabilized. On the other hand, the same steric interactions are reduced between the diamide bridge and the aryl rings in the zirconium system due to the longer  $\text{M-N}$  bonds. As a result, the aryl rings can move out of the perpendicular position. Thus, the isopropyl groups are less effective in retarding the chain termination by blocking the axial sites.

The lack of sufficient steric bulk in the zirconium diamide complex to retard the chain termination step lead us to suggest a number of modified complexes based on a general principle. The modifications involved (i) increase of the steric bulk on the diamide bridge, **13** and **14**; (ii) increase of the steric bulk on the aryl rings, **15** and **16**; (iii) the blocking of one axial position by a hydrocarbon bridge, **17** and **18**. Results from the combined QM/MM calculations indicate that the suggested modifications might be used to generate living olefin polymerization catalysts with much higher activities than the original titanium-based diamide complex suggested by McConville. Work by Piers et al. is now in progress to synthesize living zirconium-based diamide olefin polymerization catalysts similar to those suggested here.

**Acknowledgment.** This investigation has been supported by the National Sciences and Engineering Research Council of Canada (NSERC) and by the donors of the Petroleum Research Fund, administered by the American Chemical Society (ACS-PRF No. 31205-AC3), as well as by Novacor Research and Technology Corporation (NRTC) of Calgary. The Izaak Walton Killam Memorial Foundation is highly appreciated by T.Z. (Canada Council Killam Professor), L.D. (Killam postdoctoral fellowship), and T.K.W. (Killam graduate fellowship). T.K.W. also thanks NSERC and the Alberta Heritage Scholarship for graduate fellowships. The authors are greatly indebted to the staff of NRTC for the valuable discussions, especially, Drs. D. Harrison and J. McMeeking. We would also like to thank Profs. W. Piers and D. H. McConville for stimulating discussions.

**Supporting Information Available:** Tables of Cartesian coordinates and the total energy of all species mentioned in the text and a full listing of the molecular mechanics force field parameters utilized (27 pages). Ordering information is given on any current masthead page.

OM9803164